Authors' accepted manuscript.
Article published in *Construction and Building Materials*, Volume 303, 11 October 2021, 124366
The final published version is available at https://doi.org/10.1016/j.conbuildmat.2021.124366

The impact of carbon-based nanomaterial additions on the hydration reactions and kinetics of GGBS-modified cements

Chandrasekhar Bhojaraju, Michael Di Mare[1], and Claudiane M. Ouellet-Plamondon[1]

Keywords: Degree of hydration, Cementitious materials, GGBS, Nanomaterials, Graphene,

Abstract

Carbon-based nanomaterials have been identified as a viable additive to cement for making high performance binders with exceptional properties. However, on a few studies have considered the impact of these additives in combination with supplemental cementitious materials. In this work, the effect of two carbon-based nanomaterials, graphene and graphene oxide, on the hydration kinetics of cement modified with ground granulated blast furnace slag has been documented. The phase development and degree of hydration were characterized with in-situ calorimetry measurements and thermogravimetric analysis over 28 days. The results reveal a strong synergy between ground granulated blast furnace slag and graphene oxide, capable of producing cement with high degree of hydration and low cumulative heat flow. High confidence correlations, with $R^2 > 0.9$, between cumulative heat flow, degree of hydration, and compressive strength were found across the various compositions, demonstrating the importance of hydration analysis for predicting the cement properties.

1 Introduction

Concrete is use worldwide accounts for 4-8% of global CO2 emissions [1, 2]. Cement material research can increase the sustainability of cement through the development of improved volume efficiency which reduces the effective quantity of cement required. The addition of nanomaterials presents an opportunity to improve volume and cost efficiency of cement. However, the interactions between nanomaterials, such as graphene, and other common additives to cement are not well understood [3, 4]. To better characterize the chemistry of nanomaterial interactions, this work addresses a research gap in the understanding of the hydration kinetics of nanomaterial-modified cements containing blast furnace slag.

Ground granulated blast furnace slag is among the most common supplementary cementitious materials [5]. The use of such supplementary cementitious materials can improve the

environmental footprint of civil construction by reducing the cement requirements of binders. Many studies have been conducted to understand the influence of different supplementary cementitious materials on the properties of the resulting binder, including the crystalline morphology [6] and the degree of hydration [7]. Supplementary cementitious materials are typically characterized by their position on a CaO-SiO_2-Al_2O_3 ternary phase diagram, which can be used to estimate their chemical reactivity in a plain cement matrix [8]. Supplementary cementitious materials are important advancement to the development of sustainable concretes. However, to date, few studies have considered the reactivity in the presence of nanomaterials. This absence in the literature limits the capability of applying nanomaterial-modified binders to practical applications which involve supplemental cementitious materials.

The addition of nanomaterials to cements has been studied as an avenue for improving the binder performance and volume efficiency. Both graphene and graphene oxide have been shown to impact the hydration of cement and the evolution of the cement paste. Graphene oxide has been observed to promote the nucleation of calcium-silica-hydrates through a seeding effect [9, 10]. This can lower the energy barrier for the chemical evolution of the cement paste and create an accelerating effect, which has been documented [11, 12]. This has been employed to improve the sustainability of cement composites by reducing the cement requirements [13] and counteract strength reduction from undesirable recycled aggregates [14]. However, other researchers report that the hydration kinetics are unaffected by the addition of graphene oxide [15]. This inconsistency in the literature indicates the sensitivity of the nanomaterials to mix proportions and dispersion, which may influence the impact of their addition on the cement hydration [13, 16].

There is a gap in the literature on the impact of binder chemistry on the hydration of nanomaterial-modified cements. Quantifying cement hydration enables the understanding of the evolution of the cement paste and predicting the final properties of the material. The addition of supplementary cementitious materials, which is done to improve the environmental footprint of cement binders, may change the chemical compatibility of the nanoparticles and the binder matrix. In recognition of the importance of this topic, a few studies have addressed the addition of fly ash [3] and silica fume [4] to modify the binder chemistry for nanomaterial-modified cements. However, blast furnace slag has been overlooked. The present investigation addresses this research gap and a promising group of nanomaterials: graphene, and graphene oxide. To understand the

impact of these nanomaterials on the evolution of the slag-containing cement pastes, the hydration of the nano-modified cements has been studied through the following objectives:

1. Characterize the accelerating or retarding behavior of graphene and graphene oxide in the hydration of slag-containing cements.
2. Document the chemical compatibility of the nanomaterial additives with blast furnace slag.
3. Quantify the phase development in the cement paste and calculate the degree of hydration at different nanomaterial dosages and binder compositions.

This work documents the changes in the chemical reactions and kinetics of nano-modified cements containing supplementary cementitious materials to improve the understanding of the effects of these promising nanomaterial additives on cementitious binders. The work characterizes the accelerating and retarding behavior of graphene and graphene oxide additives at different dosages and in blended cements with blast furnace slag. This study supports the continued development of high performing cements with improved properties and sustainability.

2 Materials and Methodology

2.1 Materials

In the present work, ordinary Portland cement of grade 53 MPa was used to prepare the specimen. Ground granulated blast furnace slag (GGBS) was added as a replacement for the cement to form three blended binders. An additional binder without slag was taken as the reference. Water to binder ratio of 0.35 was utilized for all samples. The chemical compositions of the cement and the slag used are presented in Table 1. Each of these four binder compositions was mixed with graphene and graphene oxide nanoparticles to form nanomaterial-modified specimen. The primary characteristics of this graphene and graphene oxide nanoparticles are listed in Table 2. The nanoparticles were dispersed in aqueous suspensions with polycarboxylate superplasticizer (HRWR). For graphene, sodium cholate was added to enhance the dispersion. The size, morphology, and dispersion of the nanoparticles were confirmed by high-resolution transmission electron microscopy. Figure 1 presents a micrograph of the nanoparticles showing their topography, high crystallinity, and good dispersion. The size of the graphene and graphene oxide flakes were measured to be 150 to 200 nanometers with the thickness of 1 nanometer.

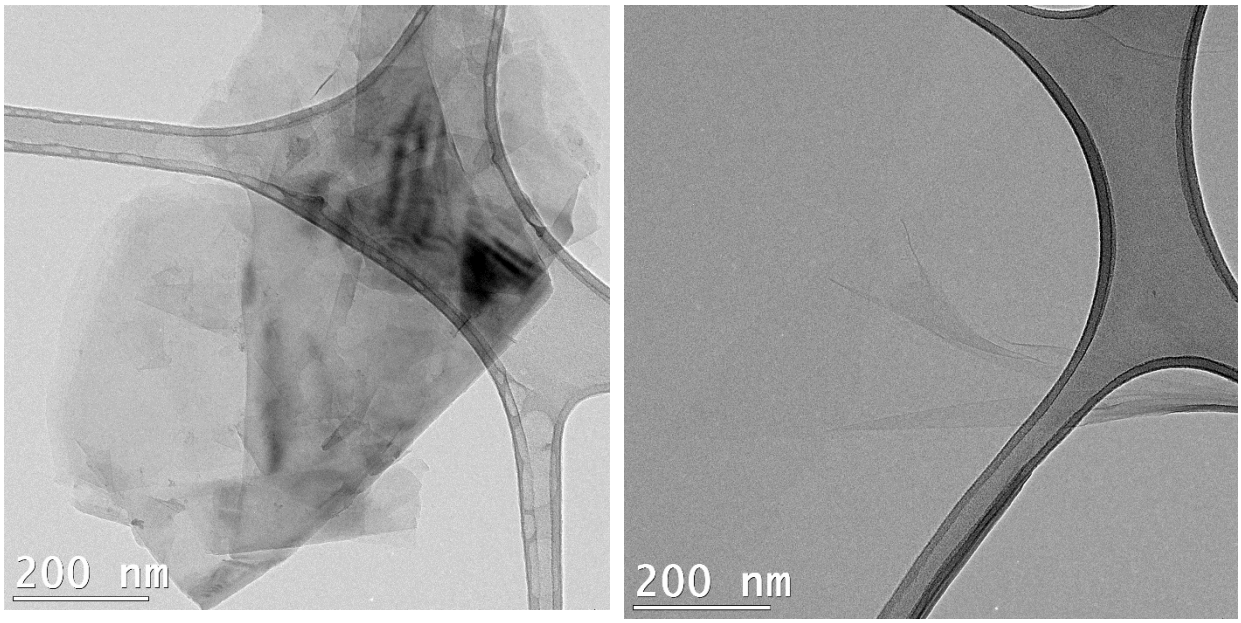

(a) (b)

Figure 1: Transmission electron microscopy images of the nanoparticles: (a) Graphene; (b) Graphene oxide

Table 1: Chemical composition of cement and ground granulated blast furnace slag (GGBS)

Parameters	Cement	GGBS
SiO_2	19.17	38.64
Al_2O_3	4.69	10.28
Fe_2O_3	3.61	2.13
CaO	61.52	35.69
MgO	2.40	8.82
SO_3	3.98	2.08
K_2O	1.06	0.78
Na_2O	0.25	0.43
TiO_2	0.25	0.56
P_2O_5	0.14	0.04
SrO	0.20	0.07
Mn_2O_3	0.05	0.31
ZnO	0.04	0.01
V_2O_5	0.01	0.11
NiO	0.00	0.02
CuO	0.02	0.01
BaO	0.01	0.06
C_3S	56.68	
C_2S	12.22	
C_3A	6.31	
C_4AF	11.00	
Loss of Ignition	2.62	0.13

2.2 Mixing and composition proportions

Four binder compositions were mixed with two dosages of each nanomaterial to form the modified cements. Ground granulated blast furnace slag was added as a replacement for the cement to make three blended binders in proportions of 15%, 30% and 45% slag by weight. The fourth binder was a reference cement without slag. The nanomaterials, graphene and graphene oxide, were tested separately at a dosage of 0.03% by weight of the binder. For the reference binder, the nanomaterials were additionally tested at 0.06% to investigate the effect of higher dosage levels.

The modified compositions are described in Table 3. The specimens are denoted by their slag content (15S, 30S, 45S), suffixed by their nanomaterial content (3G, 3GO, 6G, 6GO). In this notation, S represents slag and 3G represents 0.03% graphene. As an example, 15S3GO denotes the composition with 15% slag and 0.03% graphene oxide. The pastes were prepared by combining binder powders, gently premixed by hand, with distilled water and the nanoparticle suspensions. The mixing was conducted at 2000 rpm in a high shear mixer, shown in Figure 2, to create a homogenous mixture. The mixing was completed in three steps: (1) 1 minute of mixing, (2) 0.5-minute rest, (3) 1.5 minutes of mixing.

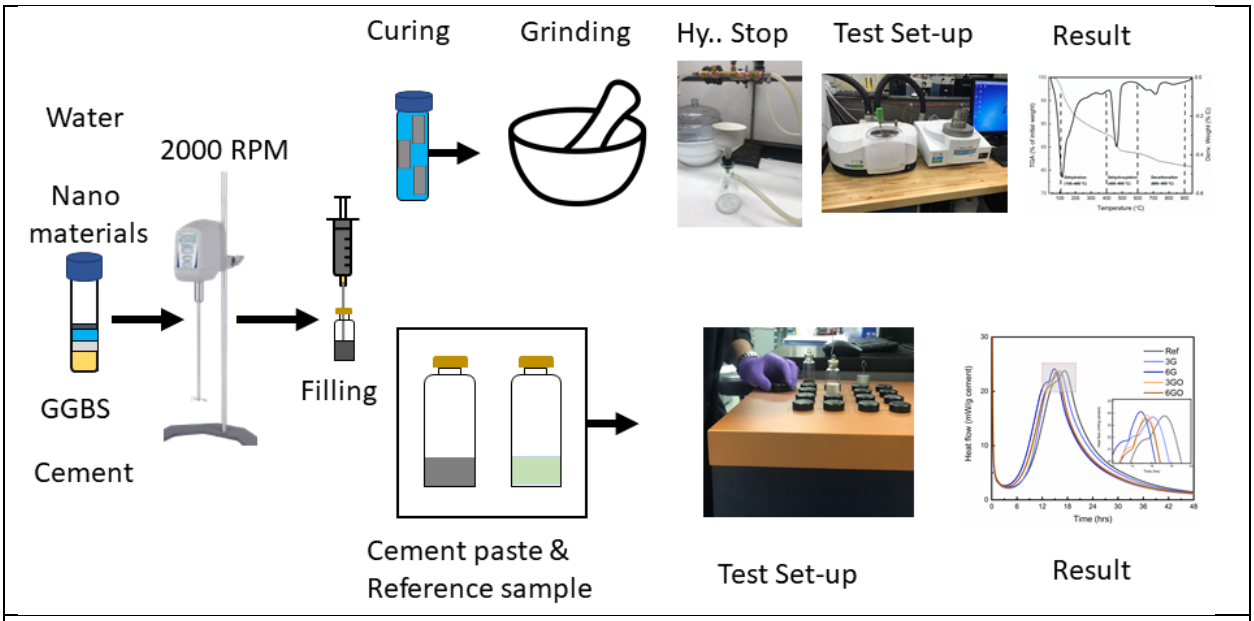

Figure 2: Experimental procedure and test set for thermogravimetric analysis and calorimetry

Table 2. Elemental composition and size of graphene and graphene oxide

Element	Carbon (%)	Oxygen (%)	Sulfur (%)	Others (%)	Particle size (μm)
Graphene	91	7	0.5	2	40
Graphene oxide	49-56	41-50	2-4	0-2	< 10

Table 3. Concrete mixture proportions.

Mixtures	Water	Cement	Sand	GGBS	Nanomaterials (% binder)		HRWR (% binder)
					Graphene	Graphene oxide	
Ref	0.35	1.0	3.0	-	-	-	1
3G	0.35	1.0	3.0	-	0.03	-	1
6G	0.35	1.0	3.0	-	0.06	-	1
3GO	0.35	1.0	3.0	-	-	0.03	1
6GO	0.35	1.0	3.0	-	-	0.06	1
15S	0.35	0.85	3.0	0.15	-		1
30S	0.35	0.70	3.0	0.30	-		1
45S	0.35	0.55	3.0	0.45	-		1
15S3G	0.35	0.85	3.0	0.15	0.03		1
30S3G	0.35	0.70	3.0	0.30	0.03		1
45S3G	0.35	0.55	3.0	0.45	0.03		1
15S3GO	0.35	0.85	3.0	0.15		0.03	1
30S3GO	0.35	0.70	3.0	0.30		0.03	1
45S3GO	0.35	0.55	3.0	0.45		0.03	1

2.3 Characterization Methods

2.3.1 Compressive Strength

To assess the compressive strength, mortars were prepared for each binder composition with binder / sand / water proportions of 1 / 3 / 0.35 by weight. Dry sieved sand of density 2,700 kg/m^3 and fineness modulus of 2.56 was used to prepare the mortars. The mortars were cast into 50-millimeter dimension cubes in agreement with ASTM C305-12 [17]. After casting, the cubes were immediately covered with a plastic film to prevent moisture loss and subsequently demolded and stored in an environmental chamber with a relative humidity greater than 95% and temperature

23±2ºC until mechanical testing. The compressive strength of the materials was measured by testing three cubes of each composition at 1, 3, 7, and 28-day intervals after casting, in accordance with ASTM C109/C19M [18]. A more detailed explanation of this process and complementary information about the development of the mechanical and rheological properties of these compositions is presented [19].

2.3.2 Isothermal Calorimetry

Isothermal calorimetry was used to investigate the in-situ hydration kinetics of the cement pastes. The heat flow was measured with a thermometric air conduction calorimeter. Approximately 7 grams of each freshly mixed paste were cast into 25.4 mm diameter glass vials, corresponding to a paste thickness of approximately 5 mm. The vials were sealed and analyzed in the calorimeter for approximately 168 hours. During the measurement, isothermal conditions of (23 ± 0.02 °C) were maintained in the measurement cells. The hydration heat flow and the cumulative hydration heat were normalized by the total binder content (cement + slag) in each sample.

2.3.3 Thermogravimetric Analysis

Thermogravimetric analysis was used to assess the changing phase composition of the cement pastes due to the hydration. In preparation for the analysis, the as-mixed cement pastes were cast into cylindrical plastic molds of inner diameter 5 millimeters. The cylinders were stored in a saturated aqueous solution of calcium at 23±2ºC to prevent leaching. At designated ages, the specimens were ground and hydration was halted through a treatment with isopropanol, diethyl ether, and vacuum drying at 40ºC for 15 minutes. The treated samples were kept under carbonation-free conditions until testing. The thermogravimetric analysis was conducted up to 950ºC at a ramp rate of 5ºC/minute.

Thermogravimetric analysis was used to determine the calcium hydroxide (CH) content within the cement paste at different times [20] and subsequently quantify the evolving degree of hydration. The degree of hydration is a numerical characterization of the hydration reactions based on the ratio of the amount of bound water in the cement paste to the stoichiometric water content of a fully reacted cement. This can be calculated from the thermogravimetric analysis by deconvolving the weight loss spectrum into finite regimes corresponding to the decomposition of

different C-S-H and C-A-S-H products. Eq. (1) was used to calculate the bound water (W_B) in the paste where Ldh, Ldx and Ldc are the weights of isopropanol dried samples at 105 °C - 400 °C, 400 °C - 600 °C and 600 °C - 1000 °C respectively. The tangent method was used to quantify the weight changes. The bound water (W_B) which indicates decomposition of hydrates such as AFm and AFt phases, and C-S-H in cement paste is computed by:

$$W_B = Ldh + Ldx + 0.41(Ldc - Ldc_a) - (m_c \times LOI_c + m_s \times LOI_s) + m_d \quad (1)$$

where m_c and m_s are the mass of cement and slag and LOI_c and LOI_s are the loss of ignition of the cement and of the slag respectively [21]. The device's drift (m_d) is a correction factor to account for the mass variation of the empty crucible at high temperature which creates a small artificial weight gain. This yields the following equation for degree of hydration:

$$\propto = \frac{W_B}{W_{B\infty} \times L_{eq}} \quad (2)$$

where $\propto$ is the degree of hydration, ultimate chemically bound water ($W_{B\infty}$) corresponding to full hydration of 1 g of the equivalent binder is similar to that of 1 g of pure cement. L_{eq} is the equivalent binder content, i.e., ($m_c + k \times m_s$). In the present investigation, 0.9 value used for k.

3 Results and Discussion

3.1 Calorimetry Results

The calorimetry analysis provides an in-situ thermal profile for characterizing the cement hydration. It enables the comparison of the relative rates of the different hydration reactions which can be identified to occur in five stages. This is shown graphically in Figure 3. In the first minutes, there is an exothermic peak (Stage I) due to the wetting of the cement particles and rapid dissolution of anhydrous phases. During this time, ettringite begins to precipitate due to the high reactivity of the aluminates and the availability of calcium sulfate. This is followed by the induction period (Stage II) and the precipitation of the main reaction products (Stage III), C-S-H and CH [22]. In the subsequent stages, the cement undergoes decaying chemical activity due to the slowing diffusion of reactants through the hardened material. Stage IV includes the sulfate depletion point at which point the dissolution of C3A and precipitation of ettringite increase [23, 24]. In Stage V, a small exothermal release corresponding to the formation of AFm from ettringite and C3A can be observed.

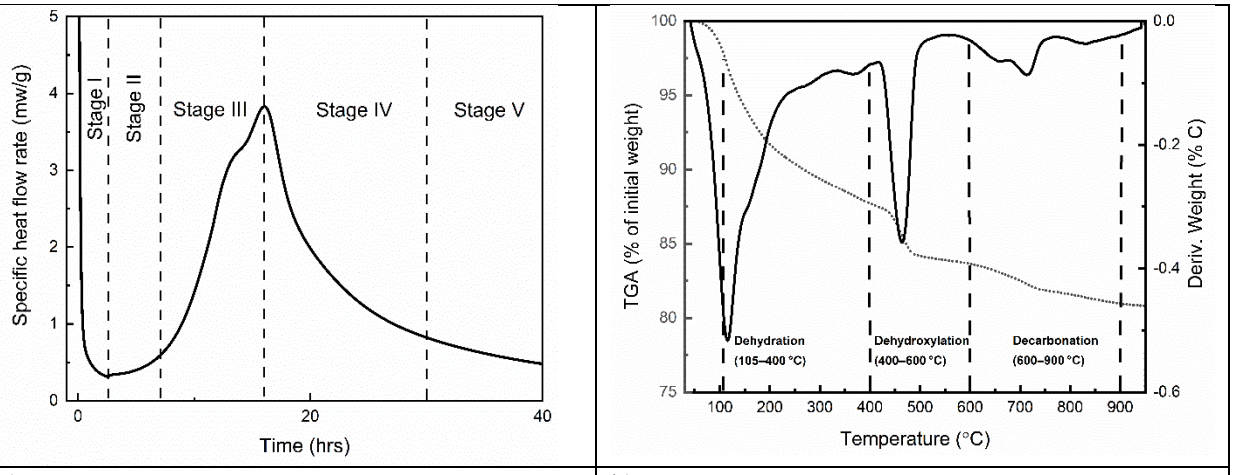

a) b)

Figure 3: Typical calorimetry and thermogravimetric analysis curves for hydrated cements

For the compositions of this study, the calorimetry analysis reveals that the addition of graphene and graphene oxide nanomaterials reduces the induction period and initiates the formation of C-S-H and CH at earlier times. This is consistent with results which have been reported by other authors [25]. This is an anticipated result which demonstrates the impact of high surface area of the nanoparticles as heterogeneous nucleation sites for cement hydration products [14]. The reactive surface area lowers the energy barrier of the hydration reactions, which improves their kinetics, resulting in the observed reduction in the induction period. In Figure 4(a), dosages of 0.03 wt% and 0.06 wt% correspond to a shift of 72 and 146 min, respectively, in the peak heat flow, whereas graphene oxide induces a shift of 110 min at both levels. Furthermore, Figure 4(a) shows that the dual-peak shape of the peak heat flow and the relative intensities of those peaks are largely unaffected by the nanomaterials. This indicates that the nucleation effect of both nanomaterials enhances the formation of C3S and C3A, corresponding to the first and second peaks, respectively, to an equal degree. However, after approximately 40 hours, the nanomaterials inhibit the hydration reaction and result in a slightly lower total heat flow, shown in Figure 4(b). This may be explained by the development of higher density cement, which exhibits a lower diffusion rate for reactant species through the hardening cement paste. For graphene oxide, this effect is slightly stronger, and the effect is more pronounced at the lower dosages of both nanomaterials.

With a high content of amorphous SiO_2, Al_2O_3 and MgO in slag, the replacement of cement with slag can change the hydration reactions. The interaction of slag and cement is known to induce

the formation of secondary C-S-H, C-A-S-H, magnesium silicate hydrate (M-S-H) and crystalline $Mg(OH)_2$ [21]. In this study, the addition of slag was observed to extend and reduce heat flow during the induction period, illustrated in the inert image in Figure 4(c). However, over an extended time frame, the impact of slag was observed to be more complicated. The addition of 15%, 30% and 45% slag caused a shift in the heat flow peak of 77, 67, and 59 minutes, respectively, but reduced the amplitude of the heat flow for all the mixes. This is consistent with observations from other authors and has been attributed to the effective increase in the water to cement ratio caused by the replacement of cement with slag [26].

In addition, during the initial setting time, a small exothermic peak is observed during the induction period. This correlates to the slag content, which suggests that it may be related to the increasing aluminium content in the binder with the addition of slag. The dual-peak shape of the reference cement is increasingly distorted with higher dosages of slag (Figure 4c). This indicates that the chemistry of hydration reactions is changing considerably, and the precipitation of C3A is being enhanced. This is an expected observation based on the greater content of aluminium in the slag, as shown in Table 1. The addition of slag is observed to dramatically reduce the total heat flow, shown in Figure 4(d), with increasing effect based on the slag content. However, this difference peaks at approximately 50 hours and diminishes at later times.

The mixture of the nanomaterials and slag in cement changes the impact of the additives on the hydration reactions. The combination of graphene oxide and slag appears to synergize to increase the effectiveness of both additives. For cement containing 15% slag, shown in Figure 4(e), the induction period was dramatically shortened, and the peak heat flow was shifted by 1.5 hours more than slag alone. However, the hydration rate was reduced after 12 hours, shown in Figure 4(f), and the difference increases over the 160-hour timespan measured, resulting in a dramatically reduced total heat flow. In contrast, the addition of graphene to slag-containing cement induces a different effect than that of either additive alone. At 15% slag, graphene appears to reverse effects of the slag, reducing the induction period but also the peak heat flow. The change in relative peak intensity suggests that graphene slows the kinetics of the C3A hydration more than C3S, resulting in a broader heat flow peak of lower intensity. However, after 50 hours, instead of further reducing the hydration rate, the total heat flow exceeds the reference cement. This suggests

an increase in the degree of hydration of this combination of slag and graphene, which will be discussed in a later section.

At 30% slag, illustrated in Figures 4(g,h), a similar trend to the 15% slag is observed. The addition of graphene oxide induces a large shift in the reaction time, which reduces the induction period and shifts the hydration peak by approximately 5 hours compared to the 30% slag cement; an effect roughly 3 times stronger than graphene alone. However, this combination has a lower heat flow roughly equivalent to that of with 15 wt% slag. In the same way, as at 15% slag cement, the addition of graphene partially reverses the effects of the slag, resulting in a hydration peak with roughly the same position and breadth as the reference. Increased heat flow through the induction period is observed, suggesting that graphene promotes the formation of ettringite during this early stage. Moreover, at later ages, the heat flow exceeds that of the cement with slag alone. However, unlike the 15% slag counterpart, the total does not exceed and only approaches that of the reference cement.

Finally, at 45% slag, graphene exhibits a similar trend while graphene oxide results in an opposite effect than was observed at lower dosages. For graphene-modified cement, shown in Figure 4(i,j), the heat flow is similar to that of the 30% slag equivalent except that the total heat flow is further reduced and the influence of graphene is diminished, resulting in final hydration only slightly greater than the slag alone. With the addition of graphene oxide, in contrast to the effects observed at 15% and 30% slag, the induction period is extended, and the heat flow is further reduced. The peak heat flow is delayed by two hours, compared to the 45% slag cement. Furthermore, in the later ages of the hydration, shown in Figure 4(j), graphene oxide further reduces the total heat flow, to a greater extent than was observed at lower dosages.

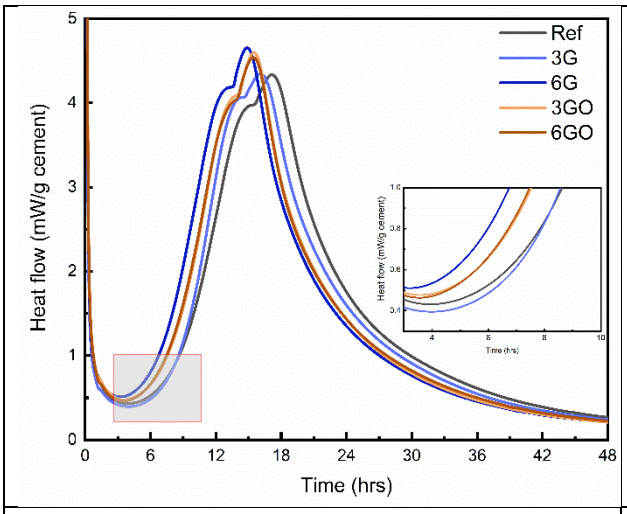
Heat flow (mW/g cement)
Time (hrs)
Ref
3G
6G
3GO
6GO

a)

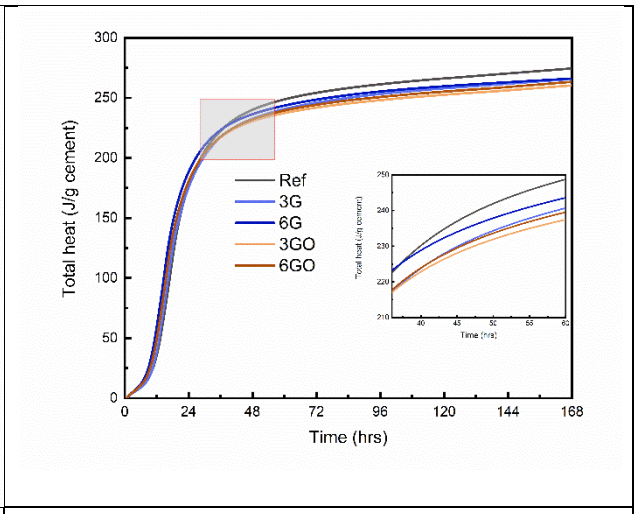
Total heat (J/g cement)
Time (hrs)
Ref
3G
6G
3GO
6GO

b)

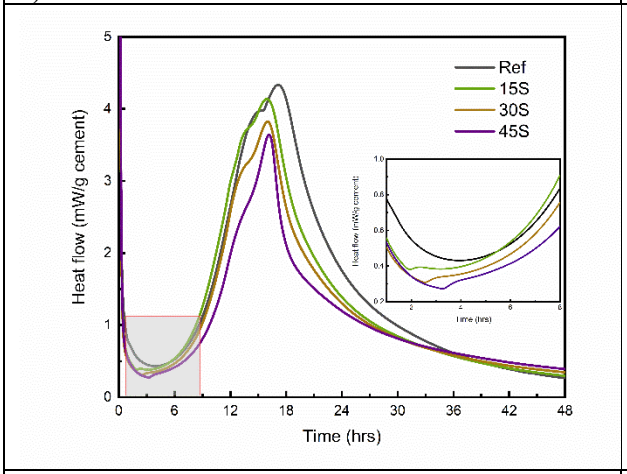
Heat flow (mW/g cement)
Time (hrs)
Ref
15S
30S
45S

c)

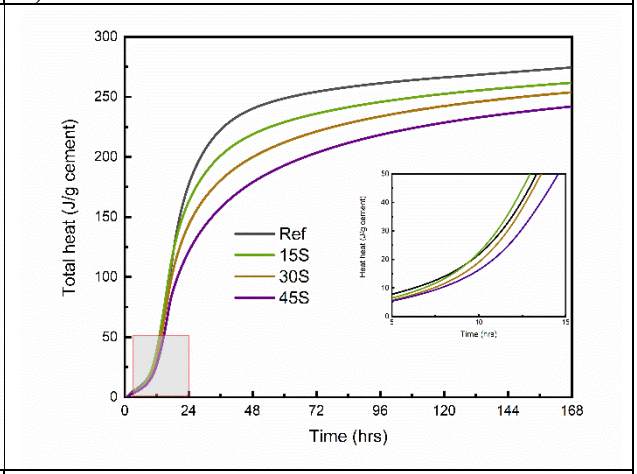
Total heat (J/g cement)
Time (hrs)
Ref
15S
30S
45S

d)

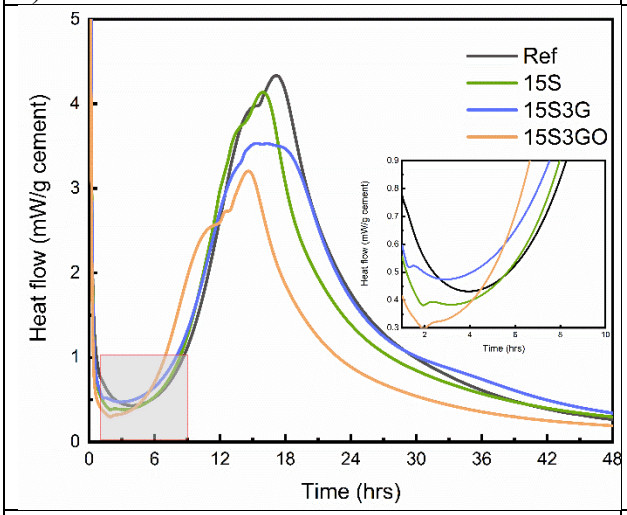
Heat flow (mW/g cement)
Time (hrs)
Ref
15S
15S3G
15S3GO

e)

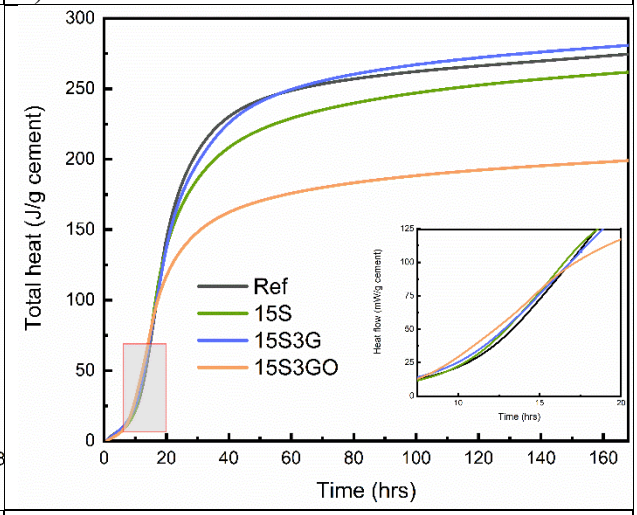
Total heat (J/g cement)
Time (hrs)
Ref
15S
15S3G
15S3GO

f)

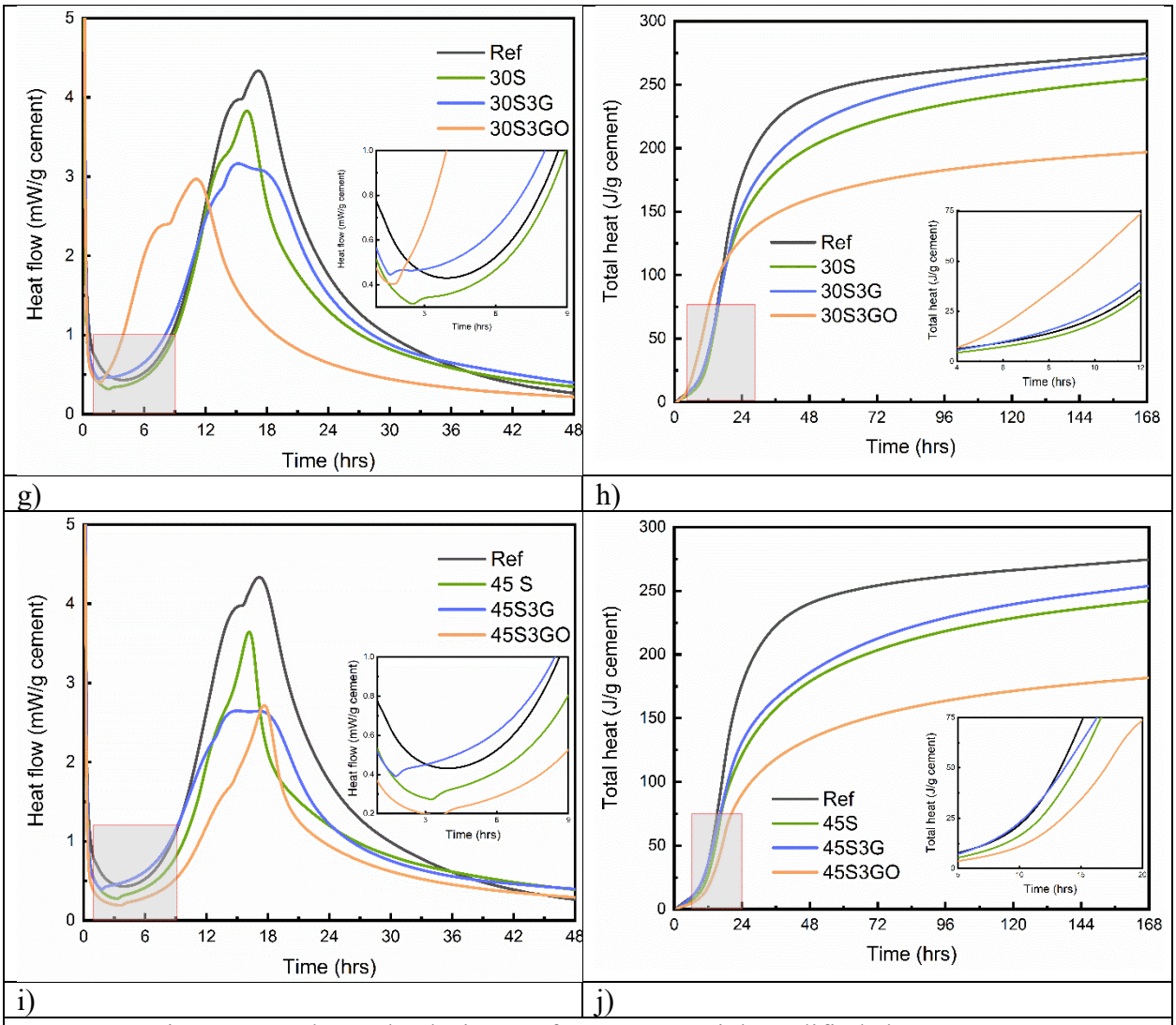

Figure 4: Isothermal calorimetry for nanomaterial-modified slag cements

3.2 Calorimetry Discussion

Calorimetry measurements represent an in-situ quantification of the hydration reaction rate in cement. As explained in a previous section, the results of this study are normalized with respect to the combined mass of cement and slag. This enables the fair comparison of materials with variable slag content. The calorimetry results can be interpreted as the total heat released during the hydration of the binder and the instantaneous heat flow which peaks before 20 hours. This peak heat flow can be compared for different combinations of slag and nanomaterials to compare the impact of the additives on the cement hydration. An increased maximum heat flow indicates that

the C3S and C3A reactions, which are strongly exothermic, occur more rapidly [22]. In contrast, a reduced maximum heat flow suggests that the additives are slowing the kinetics of the hydration.

The maximum heat flow analysis plotted against the slag content for the reference and the nanomaterial modified cement is shown in Figure 5. This analysis reveals that the nanomaterials cause the slag to increasingly reduce the hydration kinetics. As can be seen in the reference curve, the addition of slag to cement has a predictable effect on the heat flow which is strongly linear with the slag dosage [27]. The nanomaterial-modified cements exhibit a similar trend, but of a different slope which indicates that the presence of the nanomaterials enhances the reduction of the reaction kinetics. The equivalent max heat flow at 0% slag indicates that this effect is not due to the nanomaterials but instead the interaction between them and the slag [12, 28]. For the graphene, this relation is strongly linear, similar to that of the reference. However, for the graphene oxide, this trend is slightly nonlinear. This cannot be explained by the calorimetry alone but agrees with the thermogravimetric analysis and will be discussed in a later section.

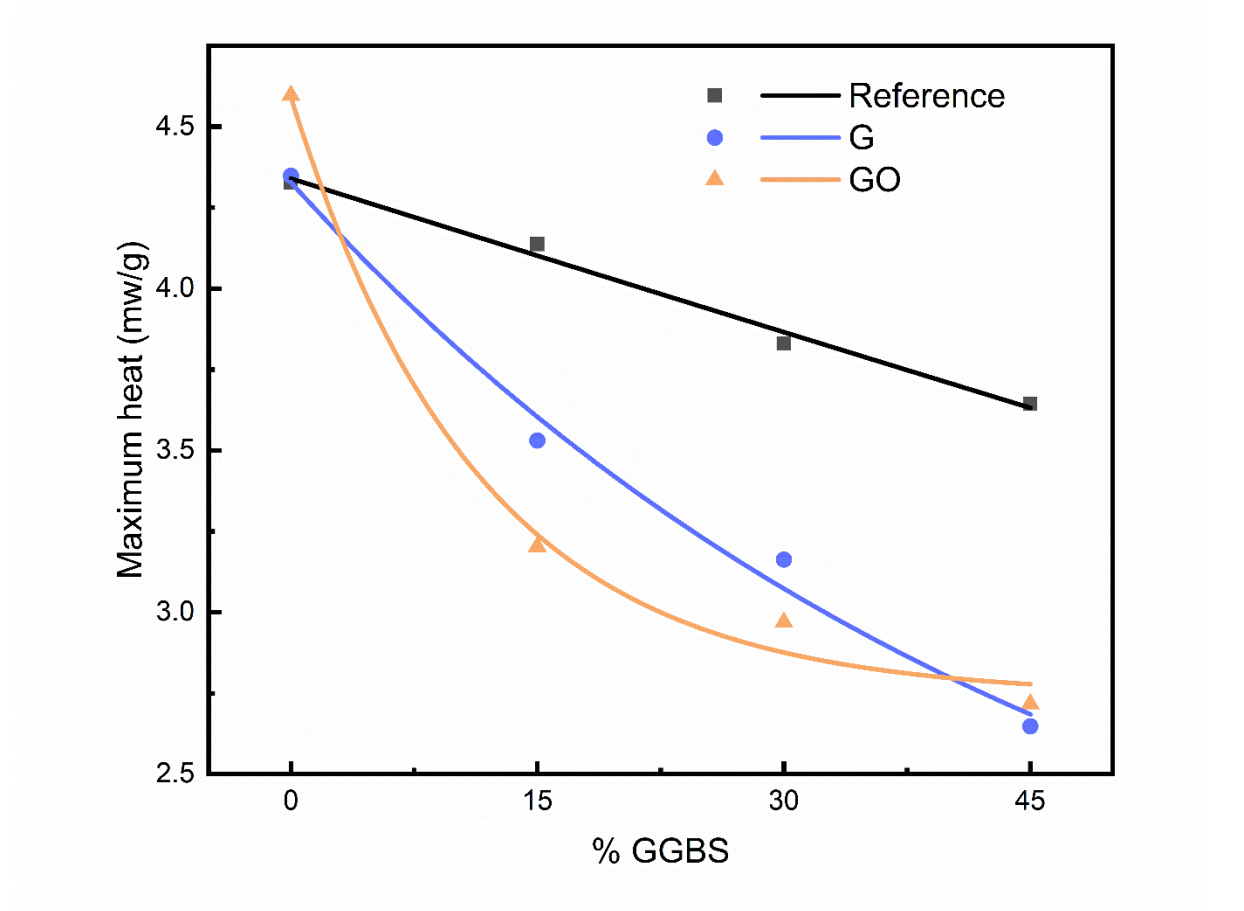

Figure 5: Maximum heat flow v. slag content for nanomaterial-modified slag cements

The calorimetry results can also be compared across all the compositions by considering the total heat flow which sums all of the heat released by the hydration reactions over the first 7 days. This is a quantitative measurement of the hydration reactions which have occurred within the cement. In Figure 6, a comparison is drawn between the total heat flow at 1, 3, and 7 days and the compressive strength of the material measured at the same time. For the reference cement and the cement containing slag and/or graphene, the results are largely linear. The correlation has high confidence with a coefficient of determination (R^2) or 0.91. This is expected for the reference and slag cement as it indicates that the compressive strength of the binder develops continuously with the progressing hydration reactions [29].

This analysis reveals the nature of the impact of the nanomaterial on the relationship between the hydration reactions and material strength. The collinearity of the graphene-modified cements with the reference cement suggests that the primary mechanism by which the graphene increases the compressive strength is by promoting the hydration reactions [30]. This relationship is unchanged by the content of slag which indicates that the addition of both slag and graphene, together or separately, does not change the chemical pathway by which the cement hydrates. Instead, only the kinetics of the reactions are affected, resulting in compressive strength, at least for the first 7 days, which are largely as expected for Portland cement which reached a comparable amount of hydration.

The analysis of the graphene oxide-modified cement shows a remarkably different interaction. For combinations of graphene oxide and slag, the relationship between the total heat and the compressive strength is markedly different. The materials achieve greater compressive strength at the same cumulative heat flow compared to the reference cement. This suggests that the strength development in the samples containing graphene oxide and slag should be attributed to a different strengthening mechanism than ordinary hydration enhancement. The results follow a new linear correlation between total heat and strength, with an R^2 of 0.96. Moreover, this new behavior does not occur for graphene oxide alone, but is independent of the slag content. This indicates that the phenomenon is unique to combinations of slag and graphene oxide and suggests that it is limited, in this range of slag contents, by the graphene oxide dosage. This unique behavior of the slag and graphene oxide cements can be explained as a change in the hydration chemistry. The resulting hydration is less exothermic which suggests that the conversion of C3A to ettringite

and the subsequent formation of AFm during Stages III and IV of the hydration are being inhibited. Thermogravimetric analysis and degree of hydration computations were completed to corroborate this result.

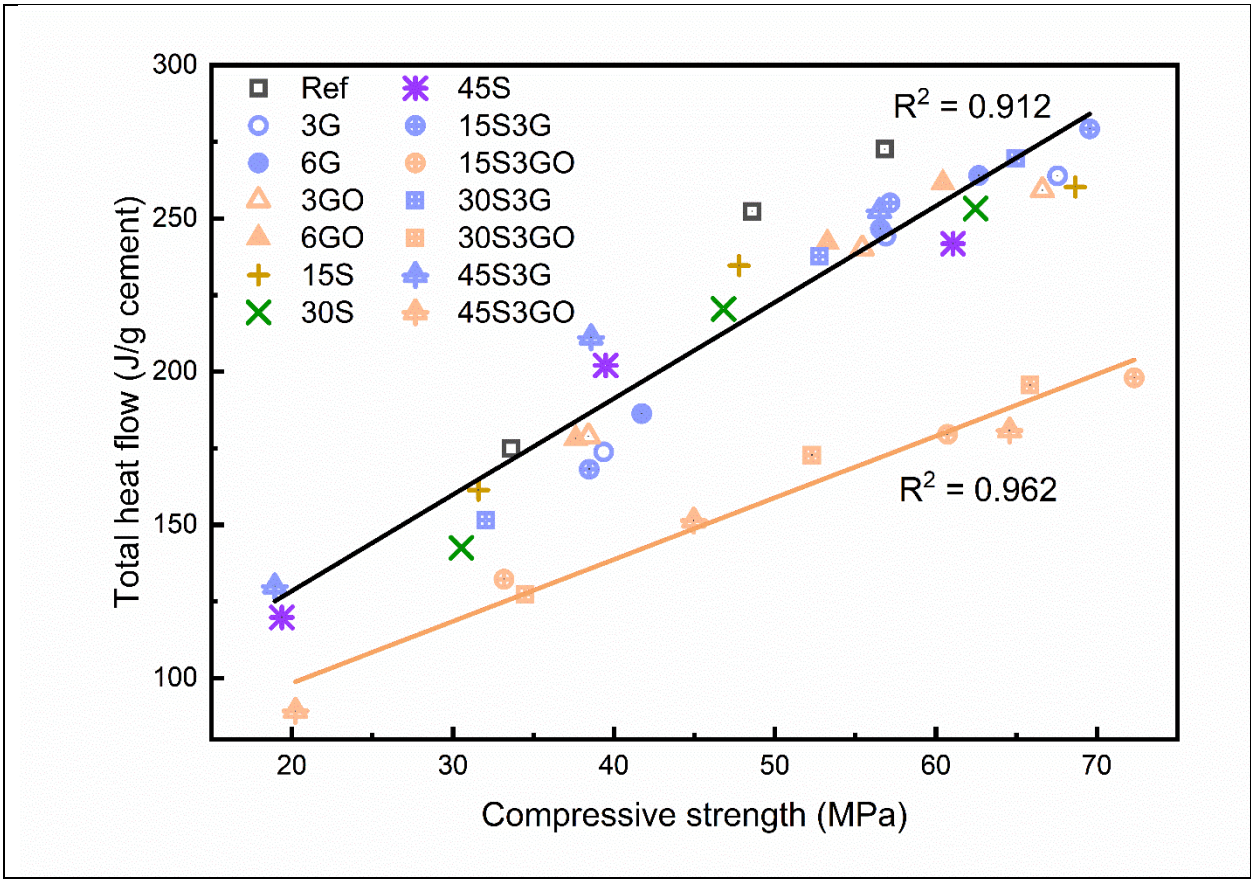

Figure 6: Total heat flow vs. compressive strength for nanomaterial-modified slag cements

3.3 Thermogravimetric Analysis Results

Thermogravimetric analysis characterizes the phase composition of the cement paste. The thermogravimetric profile can be deconvolved into a series of known chemical decompositions, indicating the contents of each known phase within the material [31]. Generally, the decomposition of cement hydrates can be divided into three major phases, as illustrated in Figure 3. The first phase involves two phenomena the evaporation of free water and the decomposition of hydrates (L_{dh} in Equation 1) which occur below 400ºC. The bound water of each between 400ºC and 600ºC, the dehydroxylation of Portlandite is dominant (L_{dx}). Above 600ºC, the decarbonation of $CaCO_3$ occurs (L_{dc}) [21]. These three decompositions can be easily quantified by thermogravimetric analysis for the determination of the phase composition. The total bound water was quantified for each mixture and is presented in Table 4. By analyzing the cement paste after 1, 3, 7 and 28 days, the evolving phase composition can be monitored.

Table 4. Total bound water (W_B) for different mixes.

	Days	**Reference**	**3G**	**3GO**	**6G**	**6GO**
Reference	1	5.18	4.46	4.90	4.96	4.31
	3	8.53	8.59	8.64	6.59	5.54
	7	6.62	6.22	6.64	6.75	6.32
	28	6.57	8.65	10.56	8.83	8.56
GGBS		**15R**	**30R**	**45R**		
	1	3.66	3.77	4.08		
	3	6.91	7.49	5.29		
	7	9.35	7.88	8.59		
	28	9.73	8.92	9.45		
G/GGBS		**15S3G**	**30S3G**	**45S3G**		
	1	4.85	4.53	3.18		
	3	7.43	7.97	5.65		
	7	6.31	5.72	5.96		
	28	10.66	9.74	8.02		
GO/GGBS		**15S3GO**	**30S3GO**	**45S3GO**		
	1	3.61	5.09	3.88		
	3	8.63	7.55	6.68		
	7	6.27	5.80	5.37		
	28	10.55	9.86	8.82		

Of principle importance is the quantification of the calcium hydroxide content in the cement. As can be seen in the first figure of each pair in Figure 7, the general trends of the thermogravimetric profiles are consistent with the addition of the nanomaterials at different levels of slag. The peaks of weight losses show no shift in temperature and vary only in magnitude between different compositions. This justifies the quantification of the calcium hydroxide ($Ca(OH)_2$) content from the dehydroxylation weight loss peak at approximately 450^oC [31]. For the addition of the nanomaterials to ordinary Portland cement, depicted in Figure 7(b), the graphene-modified cement shows an increase in $Ca(OH)_2$ after 3 days and a lower reduction in $Ca(OH)_2$ after 7 days, compared to the reference [32].

In contrast, the addition of graphene oxide has a very different effect. This nanomaterial reduces the formation of calcium hydroxide at early ages and causes the calcium hydroxide content to continue to increase up to 28 days. This suggests that graphene oxide inhibits and retards the hydroxylation of calcium in the cement paste, causing a slower phase evolution compared to the reference. This is consistent with the results of other authors, who have concluded that $Ca(OH)_2$ is reduced in graphene oxide-modified cements due to the adsorption of Ca^{2+} ions onto the surface of graphene oxide particles during the initial stages of hydration [4, 33]. The observation can also be explained by the adsorption of water onto the nanoparticle surfaces, which effectively reduces the free water content and slows the formation of $Ca(OH)_2$ [34, 35].

The content of blast furnace slag was observed to change the development of $Ca(OH)_2$ in the cement paste and the effect of the nanomaterials. The addition of slag in Portland cement has been documented in prior studies and results consistent with those works, shown in Figure 7(d), were observed here [21]. At low contents (15%) slag has an enhancing effect on the $Ca(OH)_2$ content which has been attributed, in prior studies, to the increased surface area of the slag compared to Portland cement. However, at higher levels (30% and 45%) the dilution effect reduces the $Ca(OH)_2$ levels. With the addition of the nanomaterials, the 15% and 30% slag cements show results consistent with a combination of the trends observed for the independent addition of slag and nanomaterials. As shown in Figure 7(f,h), the slag cements with graphene show an enhancement of $Ca(OH)_2$ at all ages, while the graphene oxide-modified cement shows no reduction in $Ca(OH)_2$ after 7 days.

Notably, with the addition of graphene, the 15% slag cement exhibits no further increase in $Ca(OH)_2$ which indicates that the surface area effect, which enhances the heterogeneous nucleation of this phase, is saturated. However, at 30% slag, the addition of graphene continues to improve the $Ca(OH)_2$ content which suggests that graphene may promote $Ca(OH)_2$ formation through a more complex mechanism than as simple nucleation sites. At 45% slag, a different trend was observed with the nanomaterials. The addition of graphene and graphene oxide had little impact on the development of $Ca(OH)_2$. This indicates that the dilution effect which reduces the $Ca(OH)_2$ contents in the cement pastes at higher slag contents overwhelms the enhancing effects of graphene and inhibiting effects of graphene oxide.

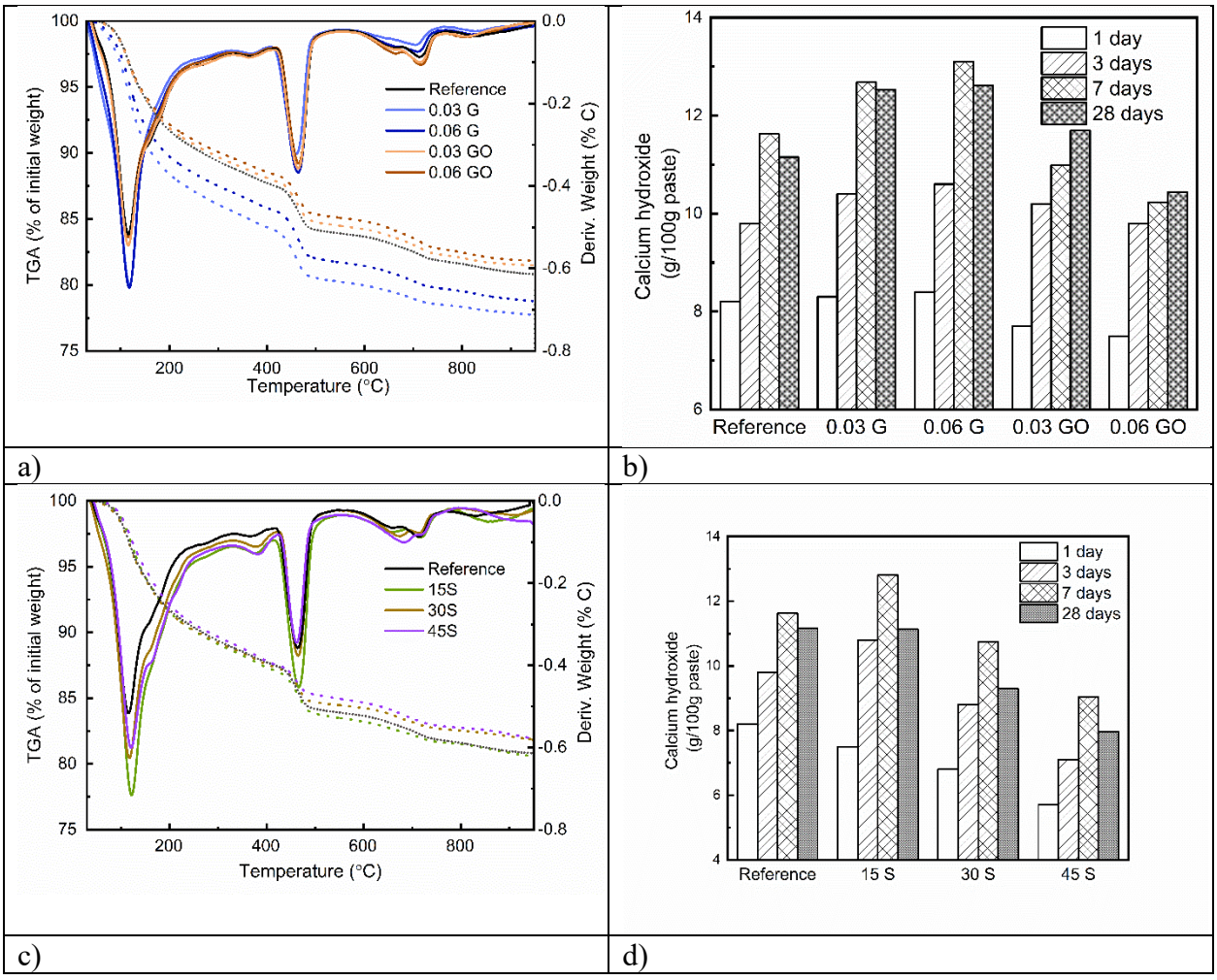

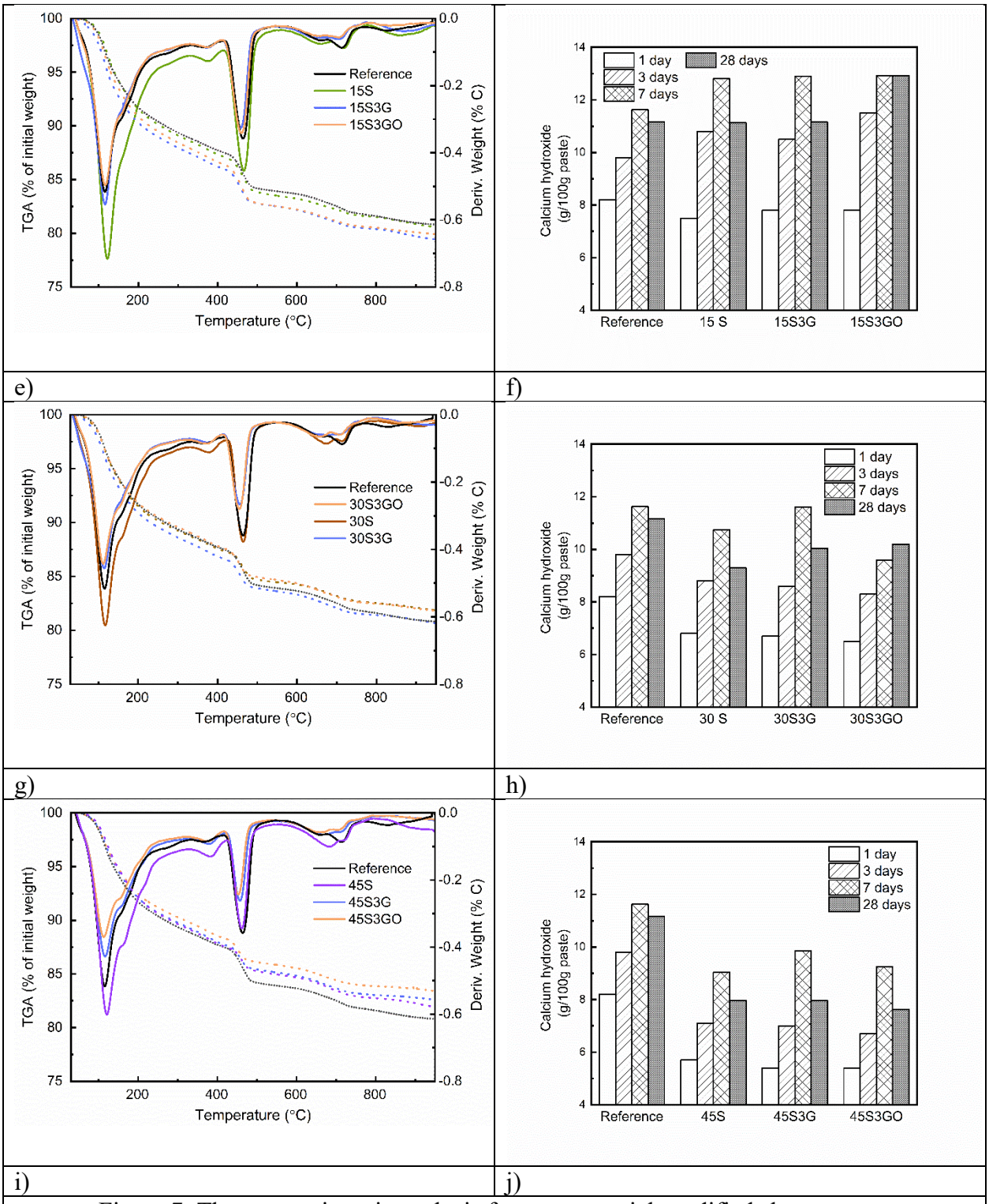

Figure 7: Thermogravimetric analysis for nanomaterial-modified slag cements

3.4 Degree of Hydration

By quantifying the thermogravimetric data into the decomposition of discrete phases, the degree of hydration at each stage of the cement's life can be calculated using Equation 2. This presents a quantification of the development of primary and secondary reaction products, such as C-S-H, AFm, and AFt, based on the consumption of free water in the composite. This value is useful for predicting the material properties of the cement, such as the compressive strength [21]. In this case, the degree of hydration is a metric of the acceleration or retardation during the first week, and the final degree of hydration achieved after 28 days, compared to the reference cement. In Figure 8(a), the impact of the nanomaterials is shown. The addition of graphene enhances the hydration at all ages [36]. This is an expected observation as it is known that nanomaterials act as nucleation points for hydration products, which increases the formation of hydrated phases [14, 37]. However, it can be seen that the higher graphene content (0.06%) results in a slightly lower final hydration. This is consistent with the calorimetry results, which observed a lower total heat flow for the 0.06% graphene cement in the first 120 hours. Graphene oxide, in contrast, induces a reduction in the degree of hydration at all ages which increases with dosage. This, again, reveals the strong difference in the chemistry of the interactions of graphene and graphene oxide with the cement matrix [38, 39].

As was observed in the $Ca(OH)_2$ calculations, the addition of blast furnace slag changes the impact of the nanomaterials in the cement composite. With the addition of slag alone, shown in Figure 8(b), the degree of hydration is reduced at 7 days and before, depending on the composition, but by 28 days the hydration surpasses that of the reference. This enhancement is inversely correlated with the slag content, with 15% slag yielding the greatest degree of hydration. Unlike in the Portland cement reference, the addition of graphene to slag-containing cement causes no significant change in the rate of hydration within 28 days. This is an unexpected observation, as it is contrary to the trend of graphene in ordinary cement and to the calorimetry results which consistently measured increased total heat flow for graphene-modified, slag-containing cement within the first 120 hours.

Furthermore, cement containing both slag and graphene oxide shows another surprising trend. In contrast to the behavior of graphene oxide reducing the hydration of normal cement, in slag-containing cements the additive behaves enhances the degree of hydration. At each dosage of

slag, the addition of graphene oxide improves the hydration of the cement at all ages. The most dramatic of these is at 15% slag, where the graphene oxide-modified cement reaches a 28-day hydration of nearly 97%. At higher slag contents, the enhancement is reduced in a similar manner to the reduction in unmodified slag cements, which is attributed to a dilution effect.

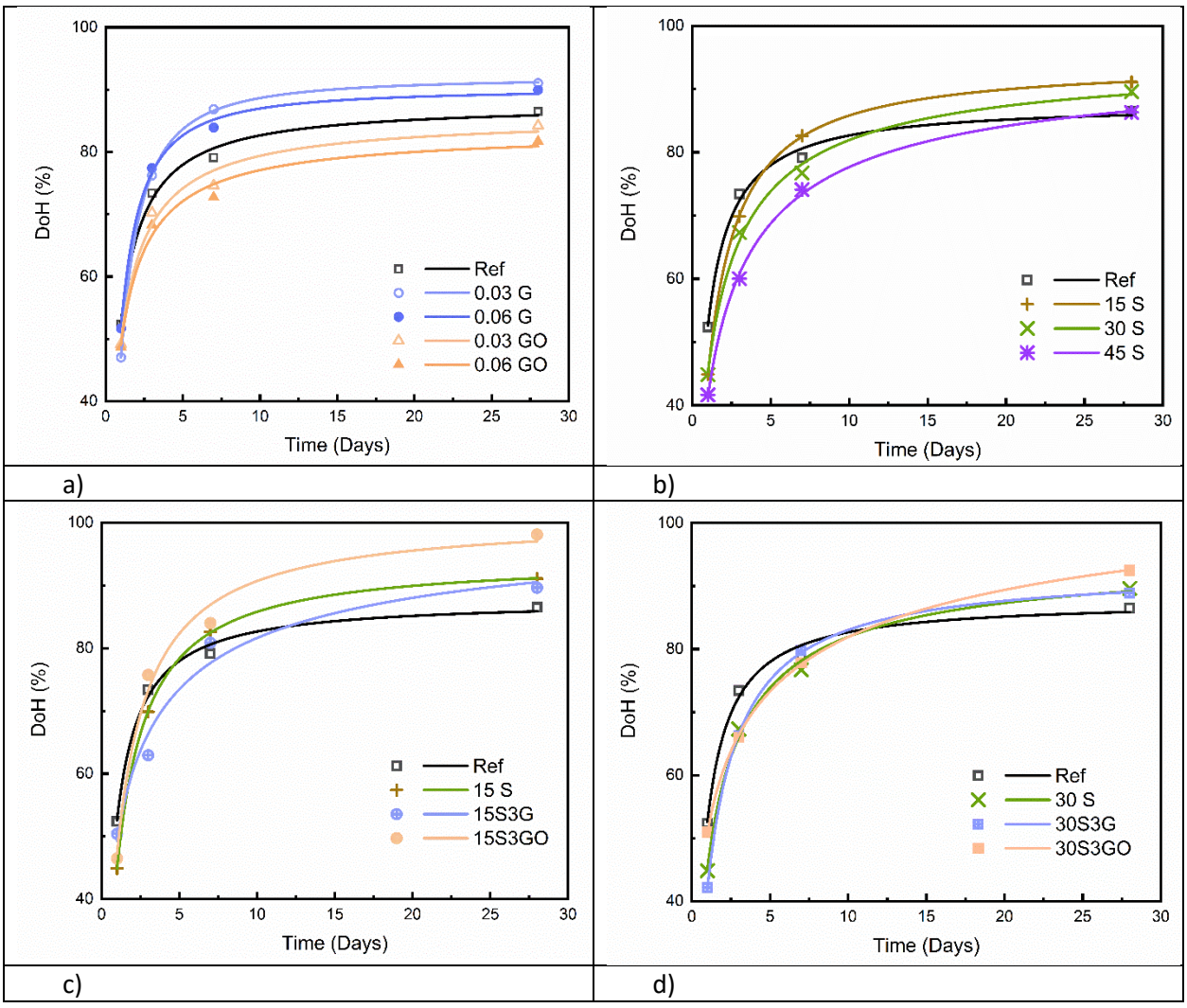

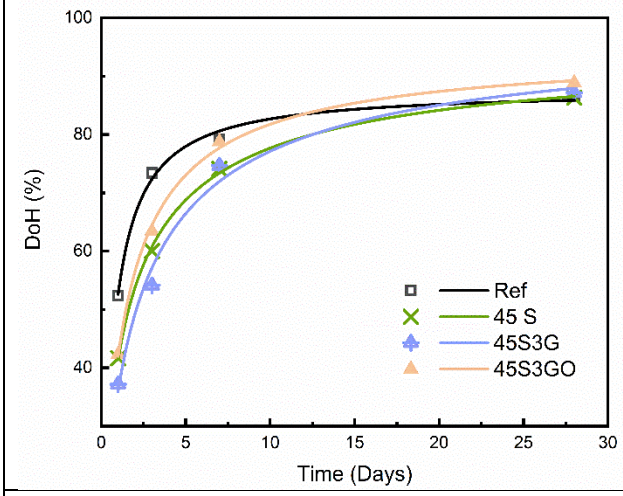

e)

Figure 8: Degree of hydration evolution over 28-day curing period

3.5 Discussion on Thermogravimetric

The degree of hydration quantifies the phase development of the cement during its hydration reactions. It is useful for comparing the structural development of different cement and can be used to predict material properties. In prior works, a positive correlation between compressive strength and degree of hydration has been reported with relatively high confidence [21]. In this study, this correlation has been tested for slag-containing and nanomaterial-modified cements. The results, presented in Figure 9, show a strong correlation between compressive strength and degree of hydration with a coefficient of determination (R^2) in excess of 0.92.

Notably, the linearity of the correlation persists despite the large volume replacement of cement with slag (up to 45%) and the strong influence of graphene and graphene oxide on the cement hydration. This indicates that the improved properties of slag- and nanomaterial-modified cement is primarily due to the development of cement of a greater degree of hydration. This observation is of particular importance to the study of graphene- and graphene oxide-modified cements because it suggests that the principal mechanism by which these nanomaterials improve the compressive strength of cement is through the degree of hydration [14, 37]. The strength improvement of nanomaterial modified cement has been attributed to various other mechanisms, including filler effects and crack deflection [14]. However, the results of this study suggest that those phenomena are dominated by the effects of heterogeneous nucleation to form cements with

a higher degree of hydration. This results in a relationship between compressive strength and degree of hydration which is largely colinear with that of unmodified Portland cement.

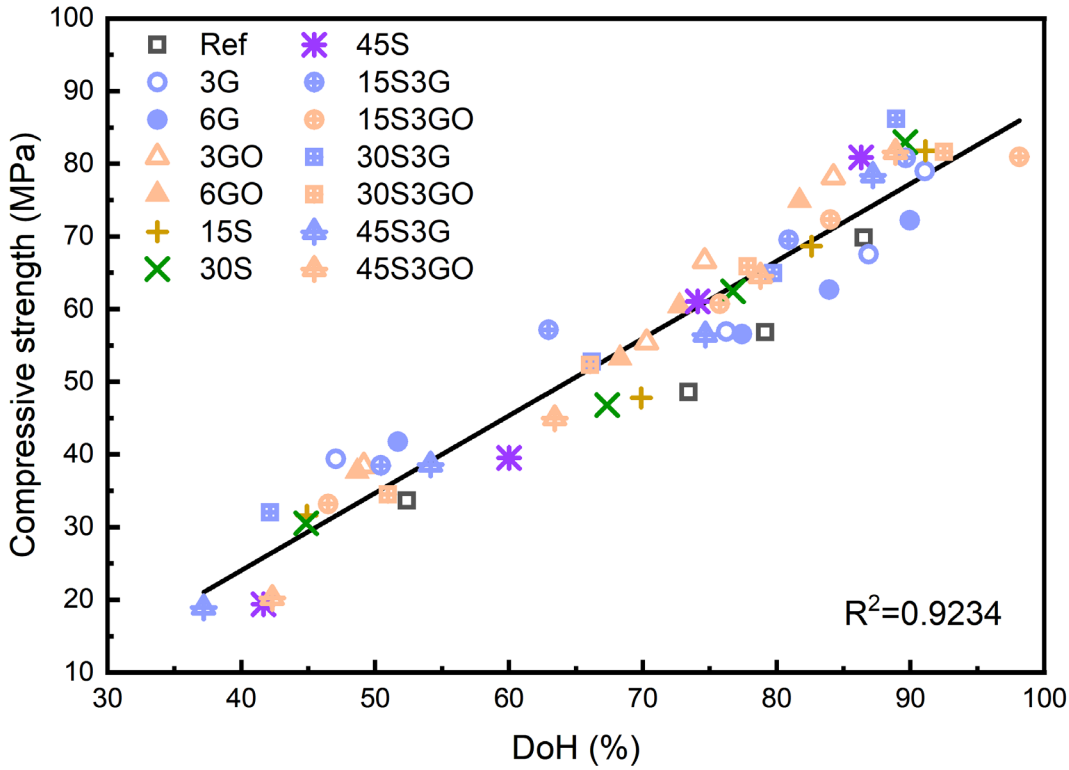

Figure 9: Compressive strength (1 to 28 days) vs. degree of hydration for nanomaterial-modified slag cements

The degree of hydration can also be correlated with the total heat flow from the calorimetry, shown in Figure 10. It is important to keep in mind in this comparison that the calorimetry is a measurement of the enthalpic heat flow from the series of hydration reactions, while the degree of hydration is a quantification of the phase composition as a percentage of completely hydrated cement. For cement synthesized with slag and graphene, the results are strongly linear with that of the reference cement. The fit has high confidence with an R^2 of 0.91. This shows that despite the apparent differences in the calorimetry and thermogravimetric analyses for these cement compositions, the ultimate relationship between the amount of heat released and the amount of hydration completed is unchanged for slag- and graphene-modified cement. This indicates that the

effects of these additives are strictly on the kinetics of the hydration and have no substantial impact on the thermodynamics or final chemistry of the cement.

In stark contrast, the results show a significant chemical change occurs for the slag cements modified with graphene oxide. These three compositions follow a different linear trend which can also be fitted with high confidence (R^2 = 0.92). This phenomenon is only observed for the compositions containing both slag and graphene oxide and suggests a unique chemical interaction between the additives. The results show that the slag and graphene oxide cement achieve a higher degree of hydration at substantially reduced total heat flows. This indicates that the thermodynamics of the hydration reactions have changed and that the resulting cement hydrates through an alternative reaction which releases less heat. The final chemistry of this cement will be different than the graphene counterparts, and that graphene oxide has a distinctly unique synergy with slag in cement. As mentioned in the discussion of the calorimetry, this may be explained by a dramatic reduction in the formation of secondary and tertiary hydration products and the formation of alternate phases which form through less exothermic reactions.

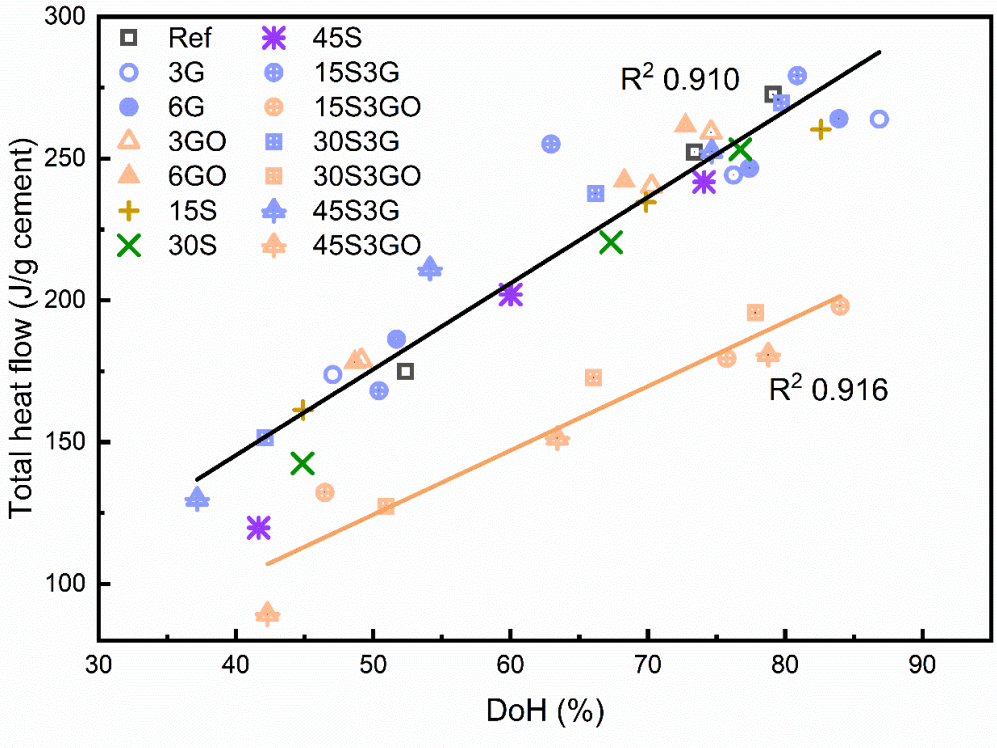

Figure 10: Total heat flow vs. degree of hydration for nanomaterial-modified slag cements

4 Conclusions

The combination of carbon-based nanomaterials and supplemental cementitious materials offers a promising avenue for binders with enhanced performance and reduced environmental footprint. This work demonstrates the need for optimization of the binder composition in conjunction with the nanomaterial type. Unexpectedly, the analysis reveals that the combination of graphene and slag retards the production of C3A more than C3S and reduces the degree of hydration compared to slag alone up to 28 days. Excellent correlations, with coefficients of determination (R^2) above 0.9, can be generated between degree of hydration, total heat flow, and compressive strength for the compositions with slag and/or graphene. The strong collinearity with the reference cement for these properties reveals that the primary mechanism by which slag and graphene, together and separately, improve the compressive strength of cement binders is through enhancing the final degree of hydration. This conclusion suggests that filler, load distributing, and other strengthening mechanisms play a smaller role than has been suggested by other authors. These results demonstrate that the hydration of cement containing slag is unimpeded by the addition of graphene and supports the development of graphene-modified cement for practical applications.

In contrast, graphene oxide shows a strongly divergent trend from the reference cement. The combination of graphene oxide and slag dramatically reduces the induction period at low slag levels and the total heat flow. Surprisingly, the thermogravimetric analysis reveals that these materials, despite the low quantity of heat released, exhibit a high degree of hydration. The relationship between compressive strength and degree of hydration is unchanged compared to the reference cement. However, a unique relationship is observed between total heat flow and degree of hydration. This indicates that cements with a combination of slag and graphene oxide hydrate through an alternative chemistry which is less exothermic. These graphene oxide-modified cement compositions achieve high final degrees of hydration and compressive strength which is unimpeded by the nanomaterial. This presents a practical advantage to applications which could benefit from lower released heat during cement hydration, such as large volume cement installations.

Acknowledgements

The Natural Sciences and Engineering Research Council (NSERC) of Canada and Quebec Centre for Advanced Materials (QCAM) from Fonds de recherche du Quebec – Nature et Technologies supported this study.

5 References

[1] R.M. Andrew, Global CO 2 emissions from cement production, 1928–2018, Earth System Science Data 11(4) (2019) 1675-1710.
[2] P. Friedlingstein, M. O'sullivan, M.W. Jones, R.M. Andrew, J. Hauck, A. Olsen, G.P. Peters, W. Peters, J. Pongratz, S. Sitch, Global carbon budget 2020, Earth System Science Data 12(4) (2020) 3269-3340.
[3] Q. Wang, S. Li, S. Pan, X. Cui, D.J. Corr, S.P. Shah, Effect of graphene oxide on the hydration and microstructure of fly ash-cement system, Construction and Building Materials 198 (2019) 106-119.
[4] X. Li, A.H. Korayem, C. Li, Y. Liu, H. He, J.G. Sanjayan, W.H. Duan, Incorporation of graphene oxide and silica fume into cement paste: A study of dispersion and compressive strength, Construction and Building Materials 123 (2016) 327-335.
[5] A. Teklay, C. Yin, L. Rosendahl, Flash calcination of kaolinite rich clay and impact of process conditions on the quality of the calcines: A way to reduce CO 2 footprint from cement industry, Applied Energy 162 (2016) 1218-1224.
[6] X. Chen, G. Wang, Q. Dong, X. Zhao, Y. Wang, Microscopic characterizations of pervious concrete using recycled Steel Slag Aggregate, Journal of Cleaner Production 254 (2020) 120149.
[7] A. Dixit, S. Gupta, S. Dai Pang, H.W. Kua, Waste Valorisation using biochar for cement replacement and internal curing in ultra-high performance concrete, Journal of Cleaner Production 238 (2019) 117876.
[8] K.C. Narang, Portland and blended cement, Ninth International Congress on the Chemistry of Cement, National Council for Cement and Building Materials, New Delhi, India, 1992, pp. 213–257.
[9] S. Sharma, N. Kothiyal, Comparative effects of pristine and ball-milled graphene oxide on physico-chemical characteristics of cement mortar nanocomposites, Construction and Building Materials 115 (2016) 256-268.
[10] Z. Lu, X. Li, A. Hanif, B. Chen, P. Parthasarathy, J. Yu, Z. Li, Early-age interaction mechanism between the graphene oxide and cement hydrates, Construction and Building Materials 152 (2017) 232-239.
[11] C. Lin, W. Wei, Y.H. Hu, Catalytic behavior of graphene oxide for cement hydration process, Journal of Physics and Chemistry of Solids 89 (2016) 128-133.
[12] W. Li, X. Li, S.J. Chen, Y.M. Liu, W.H. Duan, S.P. Shah, Effects of graphene oxide on early-age hydration and electrical resistivity of Portland cement paste, Construction and Building Materials 136 (2017) 506-514.
[13] I. Papanikolaou, N. Arena, A. Al-Tabbaa, Graphene nanoplatelet reinforced concrete for self-sensing structures–A lifecycle assessment perspective, Journal of Cleaner Production 240 (2019) 118202.
[14] W.-J. Long, D. Zheng, H.-b. Duan, N. Han, F. Xing, Performance enhancement and environmental impact of cement composites containing graphene oxide with recycled fine aggregates, Journal of Cleaner Production 194 (2018) 193-202.

[15] E. Horszczaruk, E. Mijowska, R.J. Kalenczuk, M. Aleksandrzak, S. Mijowska, Nanocomposite of cement/graphene oxide – Impact on hydration kinetics and Young's modulus, Construction and Building Materials 78 (2015) 234-242.
[16] X. Li, Y.M. Liu, W.G. Li, C.Y. Li, J.G. Sanjayan, W.H. Duan, Z. Li, Effects of graphene oxide agglomerates on workability, hydration, microstructure and compressive strength of cement paste, Construction and Building Materials 145 (2017) 402-410.
[17] C. Committee, Practice for Mechanical Mixing of Hydraulic Cement Pastes and Mortars of Plastic Consistency, ASTM International.
[18] C. Committee, Test Method for Compressive Strength of Hydraulic Cement Mortars (Using 2-in. or [50-mm] Cube Specimens), ASTM International.
[19] C. Bhojaraju, S.S. Mousavi, V. Brial, M. DiMare, C.M. Ouellet-Plamondon, Fresh and hardened properties of GGBS-contained cementitious composites using graphene and graphene oxide, Construction and Building Materials 300 (2021) 123902.
[20] V. Brial, H. Tran, L. Sorelli, D. Conciatori, C.M. Ouellet-Plamondon, Evaluation of the reactivity of treated spent pot lining from primary aluminum production as cementitious materials, Resources, Conservation and Recycling 170 (2021) 105584.
[21] W. Deboucha, N. Leklou, A. Khelidj, M.N. Oudjit, Hydration development of mineral additives blended cement using thermogravimetric analysis (TGA): Methodology of calculating the degree of hydration, Construction and Building Materials 146 (2017) 687-701.
[22] H.F. Taylor, Cement chemistry, Thomas Telford London1997.
[23] W. Lerch, The influence of gypsum on the hydration and properties of Portland cement pastes, 2008.
[24] C. Hesse, F. Goetz-Neunhoeffer, J. Neubauer, A new approach in quantitative in-situ XRD of cement pastes: Correlation of heat flow curves with early hydration reactions, Cement and Concrete Research 41(1) (2011) 123-128.
[25] T.S. Qureshi, D.K. Panesar, Impact of graphene oxide and highly reduced graphene oxide on cement based composites, Construction and Building Materials 206 (2019) 71-83.
[26] H. Yang, M. Monasterio, H. Cui, N. Han, Experimental study of the effects of graphene oxide on microstructure and properties of cement paste composite, Composites Part A: Applied Science and Manufacturing 102 (2017) 263-272.
[27] W. Sha, G. Pereira, Differential scanning calorimetry study of hydrated ground granulated blast-furnace slag, Cement and concrete research 31(2) (2001) 327-329.
[28] L. Zhao, X. Guo, Y. Liu, C. Ge, L. Guo, X. Shu, J. Liu, Synergistic effects of silica nanoparticles/polycarboxylate superplasticizer modified graphene oxide on mechanical behavior and hydration process of cement composites, RSC advances 7(27) (2017) 16688-16702.
[29] A. Attari, C. McNally, M.G. Richardson, A combined SEM–Calorimetric approach for assessing hydration and porosity development in GGBS concrete, Cement and concrete composites 68 (2016) 46-56.
[30] G. Jing, Z. Ye, X. Lu, P. Hou, Effect of graphene nanoplatelets on hydration behaviour of Portland cement by thermal analysis, Advances in Cement Research 29(2) (2017) 63-70.
[31] T. Kim, J. Olek, Effects of sample preparation and interpretation of thermogravimetric curves on calcium hydroxide in hydrated pastes and mortars, Transportation research record 2290(1) (2012) 10-18.
[32] Y. Lin, H. Du, Graphene reinforced cement composites: A review, Construction and Building Materials 265 (2020) 120312.
[33] S. Park, K.-S. Lee, G. Bozoklu, W. Cai, S.T. Nguyen, R.S. Ruoff, Graphene oxide papers modified by divalent ions—enhancing mechanical properties via chemical cross-linking, ACS nano 2(3) (2008) 572-578.

[34] Y. Shang, D. Zhang, C. Yang, Y. Liu, Y. Liu, Effect of graphene oxide on the rheological properties of cement pastes, Construction and Building Materials 96 (2015) 20-28.
[35] F. Babak, H. Abolfazl, R. Alimorad, G. Parviz, Preparation and Mechanical Properties of Graphene Oxide: Cement Nanocomposites, The Scientific World Journal 2014 (2014) 276323.
[36] T.S. Qureshi, D.K. Panesar, Nano reinforced cement paste composite with functionalized graphene and pristine graphene nanoplatelets, Composites Part B: Engineering (2020) 108063.
[37] S. Nazar, J. Yang, B.S. Thomas, I. Azim, S.K.U. Rehman, Rheological properties of cementitious composites with and without nano-materials: A comprehensive review, Journal of Cleaner Production (2020) 122701.
[38] X. Li, Z. Lu, S. Chuah, W. Li, Y. Liu, W.H. Duan, Z. Li, Effects of graphene oxide aggregates on hydration degree, sorptivity, and tensile splitting strength of cement paste, Composites Part A: Applied Science and Manufacturing 100 (2017) 1-8.
[39] G. Xu, S. Du, J. He, X. Shi, The role of admixed graphene oxide in a cement hydration system, Carbon 148 (2019) 141-150.